Anisotropy in shale from Mont Terri

Hans-Rudolf Wenk and Marco Voltolini, University of California, Berkeley, USA
Hartmut Kern, Institut für Geowissenschaften, Universität, Kiel, Germany
Till Popp, Institut für Gebirgsmechanik GmbH, Leipzig, Germany
Martin Mazurek, Institut für Geologie, Universität, Bern, Switzerland

Anisotropy of shales is the subject of this report, and we use an example of the Jurassic Opalinus Clay from Mont Terri (Switzerland) that is being investigated in the context of radioactive waste disposal. The study is targeted at the geomechanical characterization of shale by laboratory testing. The overall aim is to improve the constitutive material laws and their application in numerical models.

Argillaceous rocks are good candidates for radioactive waste storage because of their very low permeability and high capacity to retain radionuclides, essential characteristics to isolate radionuclides released from the biosphere. For this study, we chose a sample from the Mont Terri Rock Laboratory (Canton Jura, Switzerland), which is operated by an international consortium concerned with radioactive waste disposal. Consortium members include, among others, Nagra (Nationale Genossenschaft für die Lagerung radioaktiver Abfälle, Switzerland) and BGR (Bundesanstalt fur Geowissenschaften und Rohstoffe, Germany) who provided the sample.

A major factor contributing to shale anisotropy is preferred orientation (or texture) of clay minerals attained during sedimentation and compaction. We quantified these preferred orientation patterns with a novel synchrotron X-ray diffraction technique and, on the same samples, determined ultrasonic wave speeds as a function of pressure and direction with a triaxial loading apparatus. Results from the mineralogical, textural, and seismic-wave analysis were then compared.

The Mont Terri underground laboratory consists of a dedicated tunnel section that branches off an existing highway tunnel in the Jura Mountains. The Opalinus Clay was deposited in the Jurassic and was subjected to two successive stages of burial, in the Cretaceous and in the Tertiary, with a maximum burial depth of about 1350 m (Mazurek et al., 2006). Folding of the mountain belt occurred between 10.5 and 3 million years ago. The sample used here originates from a depth of about 270 m below the surface and comes from the shaly facies that occurs in the stratigraphically lowermost portion of the Opalinus Clay.

The homogeneous sample was divided into three parts. One was investigated for mineralogical composition and microstructure at the University of Bern (Switzerland). Slabs of the sample, 20 × 20 × 2 mm^3, cut more or less perpendicular to the macroscopic bedding, were investigated for preferred orientation at Berkeley. A cube, with an edge length of 43 mm, was used for the ultrasonic velocity measurements at the rock deformation laboratory of Kiel University (Germany).

The Opalinus Clay is a fairly homogeneous formation of considerable extent and thickness in the Molasse Basin of Switzerland. With the exception of quartz-rich, silty lenses, Opalinus Clay is not cemented. The mineralogical composition of the sample was analyzed by standard X-ray powder diffraction (XRD) and coulometric techniques and with a Rietveld refinement of synchrotron data. The sample is 20% quartz, 6% calcite, 2% K-feldspar, and 70% clay minerals. The calcite is concentrated in shell fragments. Accessory phases include albite (1.5%), pyrite (1.6%), siderite (1.2%), dolomite/ankerite (1%), and organic matter (Corg = <0.5%). The clay minerals are illite (38%) and mixed illite/smectite (4.5%), kaolinite (21%), and chlorite (6%). With conventional mineralogic methods, including XRD and ethylene glycol solvation, it is established that clay minerals consist of an ordered illite/smectite mixed-layer phase with 70–85% illite layers, well crystallized illite (probably including a proportion of detrital mica), and poorly crystallized illite with a broad 001 diffraction peak at 10 Å. A sharp peak at 14.3–14.5 Å indicates well-crystallized chlorite, and a limited shift upon solvation is interpreted to be due to <10% interstratified smectite layers. Physical porosity was determined from measurements of the bulk-dry density and grain density of the sample, 2.28 and 2.70 g/cm^3, respectively. This established a porosity of 15.6%.

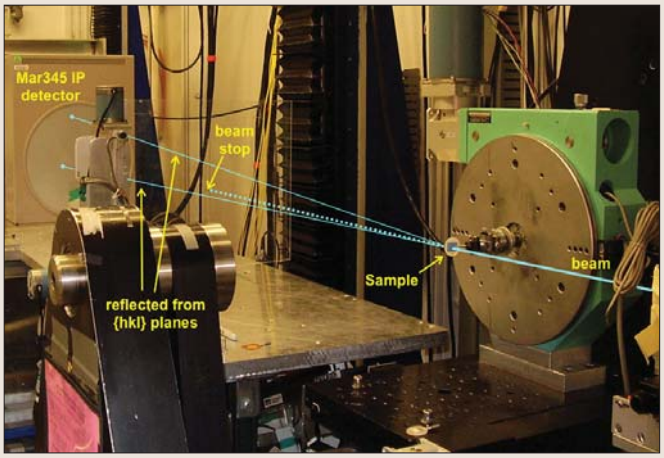

Figure 1. *Experimental setup at the Advanced Photon Source (beamline 11–ID-C) for the synchrotron X-ray texture measurements.*

For texture analysis, we relied on diffraction images obtained with hard X-ray synchrotron diffraction. The advantages of a synchrotron X-ray source are high brilliance, a focused beam, and, for hard X-rays (high energy, short wavelengths), high-sample penetration without major absorption. We used the high-energy beamline BESSRC 11-ID-C at the Advanced Photon Source of Argonne National Laboratory, with a monochromatic wavelength of 0.107877Å. Beam size was 1 mm. The sample slabs were mounted on a metal rod approximately perpendicular to the bedding plane and parallel to the horizontal axis of a goniometer (Figure 1). Diffraction images were recorded with a Mar345 image plate detector (3450 × 3450 pixels) mounted about 2 m behind the sample. During data collection, the sample was translated parallel to the horizontal axis over five spots in 2-mm increments to obtain a representative average. It was also tilted around the horizontal axis in 15° increments from -45° to 45°, producing seven images. This improves the pole figure coverage.

A typical diffraction image (Figure 2) displays a large number of Debye rings, corresponding to different lattice planes and different phases. The intensity variations along many rings immediately reveal the presence of texture. This becomes even more apparent if the image is "unrolled" and

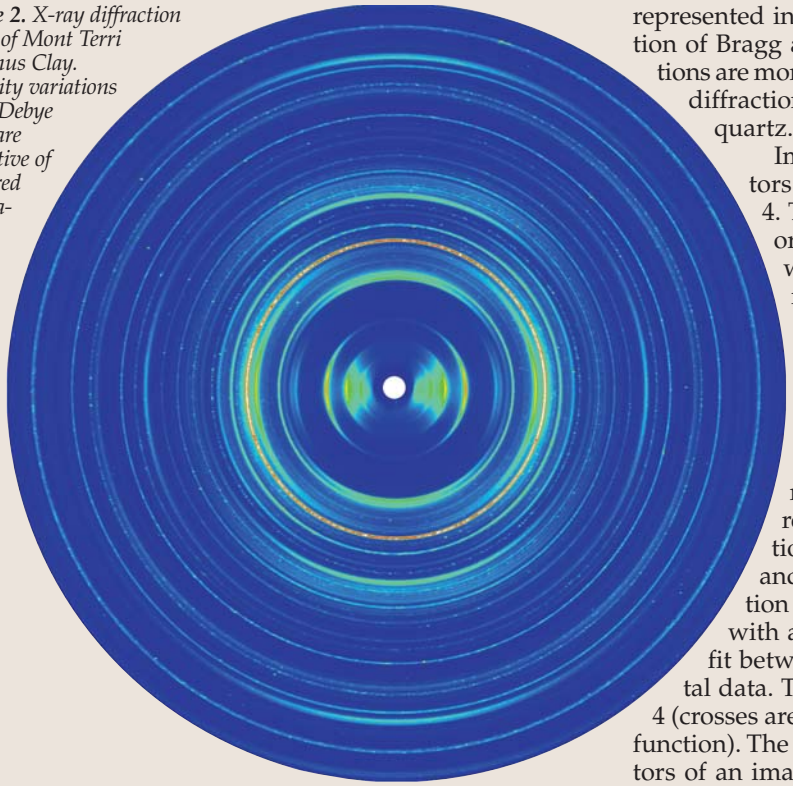

Figure 2. *X-ray diffraction image of Mont Terri Opalinus Clay. Intensity variations along Debye rings are indicative of preferred orientation.*

represented in a 3D image of intensity (counts) as a function of Bragg angle 2θ and azimuth (Figure 3). The variations are more pronounced for sheet silicate phases (at low diffraction angles) and less for calcite and particularly quartz.

Images were integrated over 10° azimuthal sectors to obtain spectra such as the two in Figure 4. The 36 spectra, each representing differently oriented lattice planes, from all seven images, were then used simultaneously in the Rietveld refinement. The crystallographic Rietveld method uses a continuous spectrum and is particularly adapted to polymineralic samples with many overlapping peaks as illustrated by the lines below the spectra in Figure 4. The diffraction spectrum is expressed by a model function that depends on many parameters, including instrument geometry and resolution, scattering background, weight fractions of phases present, their crystal structure and microstructure, and the preferred orientation patterns. These parameters are then refined with a least-squares method to obtain an optimal fit between the model function and the experimental data. This fit is very good for the spectra in Figure 4 (crosses are experimental data and the line is the model function). The two spectra are from different azimuthal sectors of an image. The top one (green) is for lattice planes

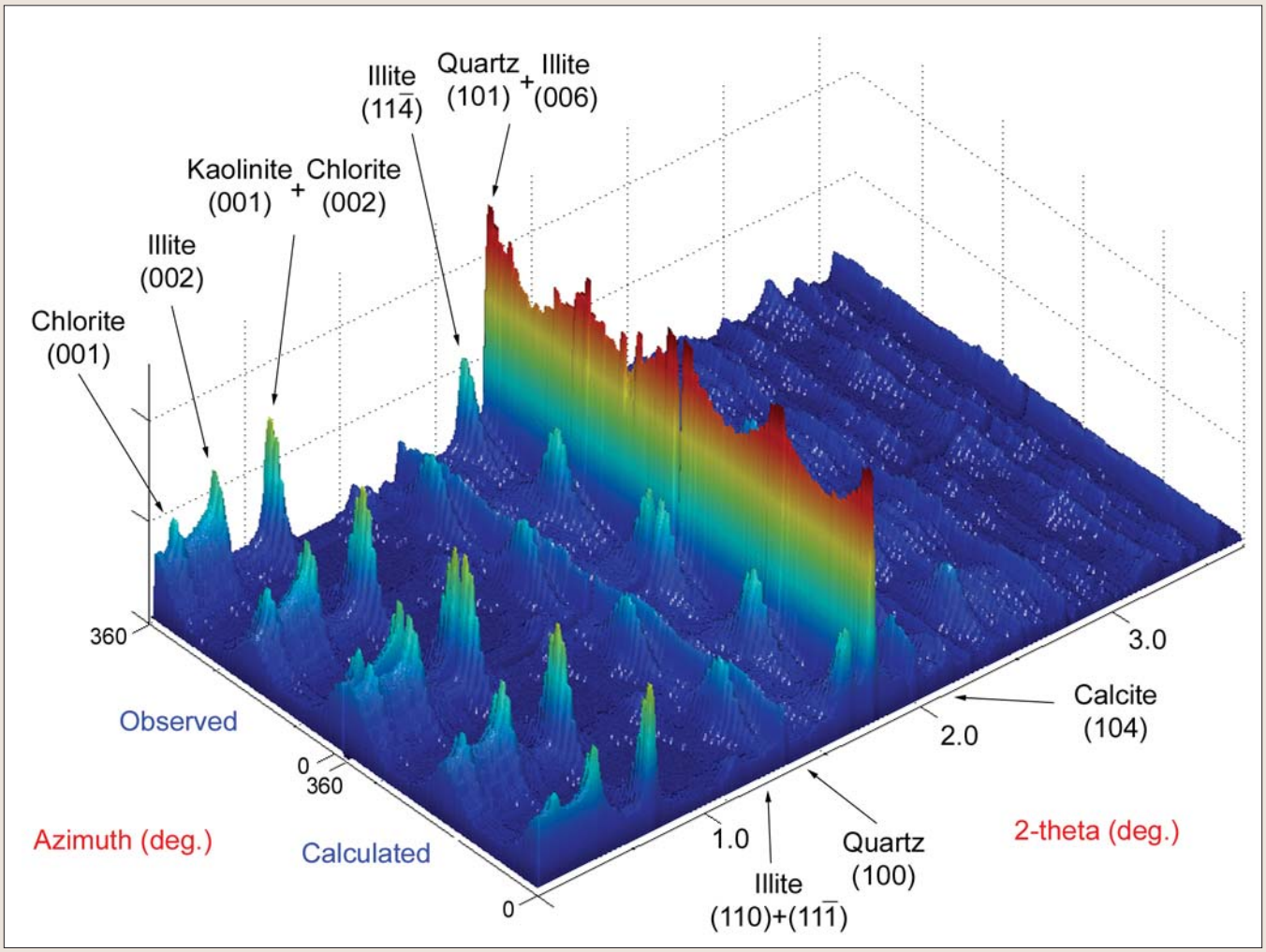

Figure 3. *3D representation of an "unrolled" image such as in Figure 2 (same color pattern is used). Some diffraction peaks are identified. The image compares observed intensities with calculated intensities based on the Rietveld refinements.*

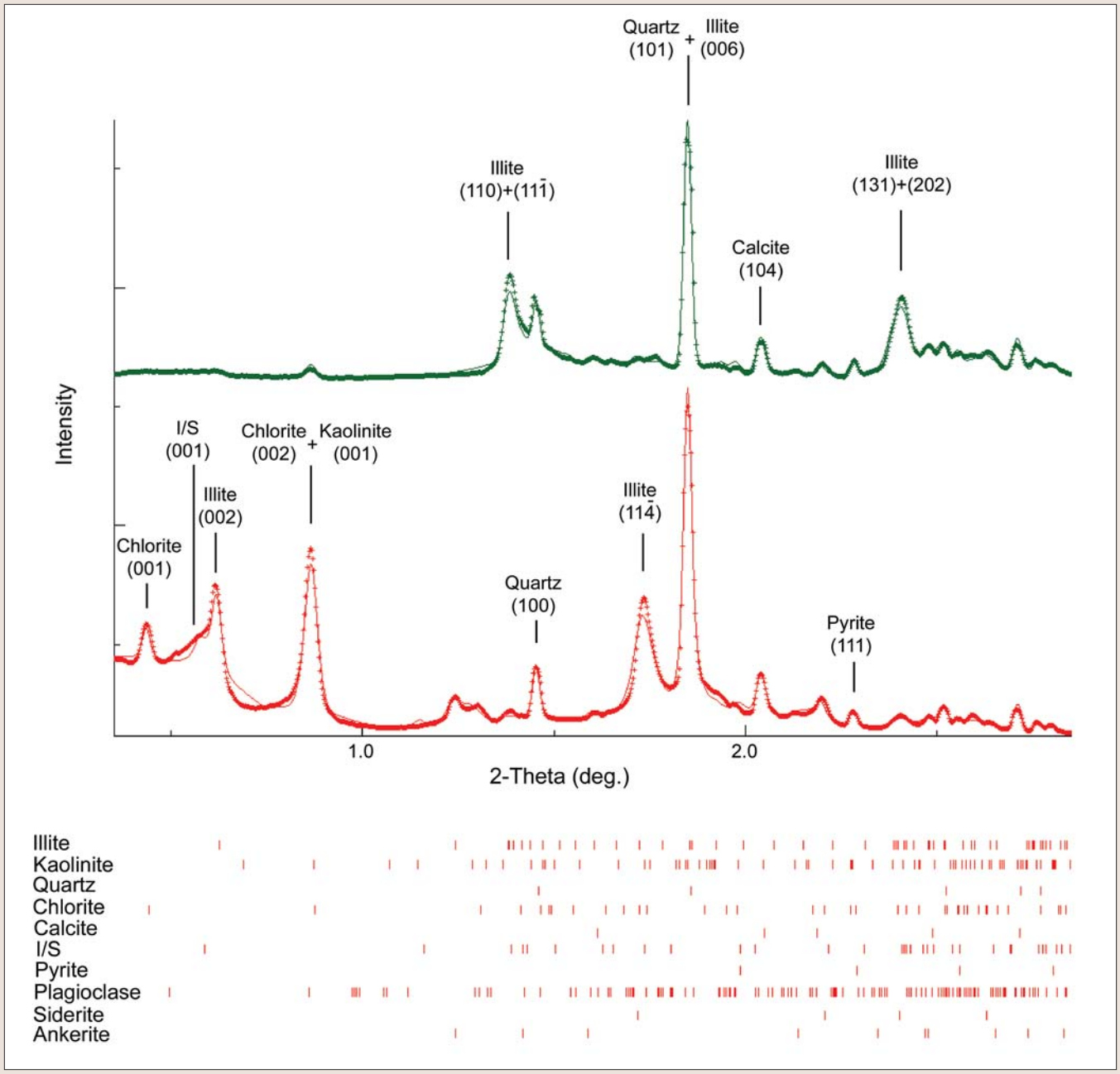

Figure 4. *Two integrated X-ray diffraction patterns. The top (green) is for diffraction on lattice planes perpendicular to the bedding and the bottom (red) for lattice planes parallel to the bedding. Some peaks are indexed. Ten phases have been used and texture patterns were deconvoluted for the six major phases.*

perpendicular to the bedding and the bottom one (red) is for lattice planes parallel to the bedding. The relative changes in peak intensities are due to texture and are the main interest in this study. For example intensities of (002) reflections of illite and (001) of kaolinite are much higher for lattice planes parallel to the bedding. For the Rietveld refinement, we used the program MAUD (Material Analysis Using Diffraction), a code written in Java.

For illite, kaolinite, illite-smectite, chlorite, quartz, and calcite, orientation distributions (OD) were refined. The three-dimensional OD defines the orientations of crystallites relative to sample coordinates. From the ODs, pole figures were calculated that display, in a spherical projection, the orientation of crystal directions, for example poles to lattice planes 001. We projected pole figures on the bedding plane and express pole densities in multiples of a random distribution (mrd). The 001 pole figures in Figure 5 illustrate strong textures for illite (6.1 mrd) and kaolinite (6.3), a weaker texture for illite-smectite (3.1), chlorite (4.4), calcite (4.4), and a random orientation distribution for quartz. Pole figures are nearly axially symmetric with a (001) maximum perpendicular to the bedding plane and no significant constraint on the orientation of *a*-axes; i.e., they are randomly distributed around (001) poles in the bedding plane, as illustrated by (100) pole figures. Preferred orientation of sheet silicates was attained during sedimentation and compaction. Interestingly, kaolinite has a sharp (001) peak on a broad distribution of randomly oriented crystallites, whereas illite shows a more Gaussian distribution. The alignment of calcite may be due to shell fragments with biogenic texture.

Texture patterns are important in the context of anisotropy of macroscopic physical properties. In the case

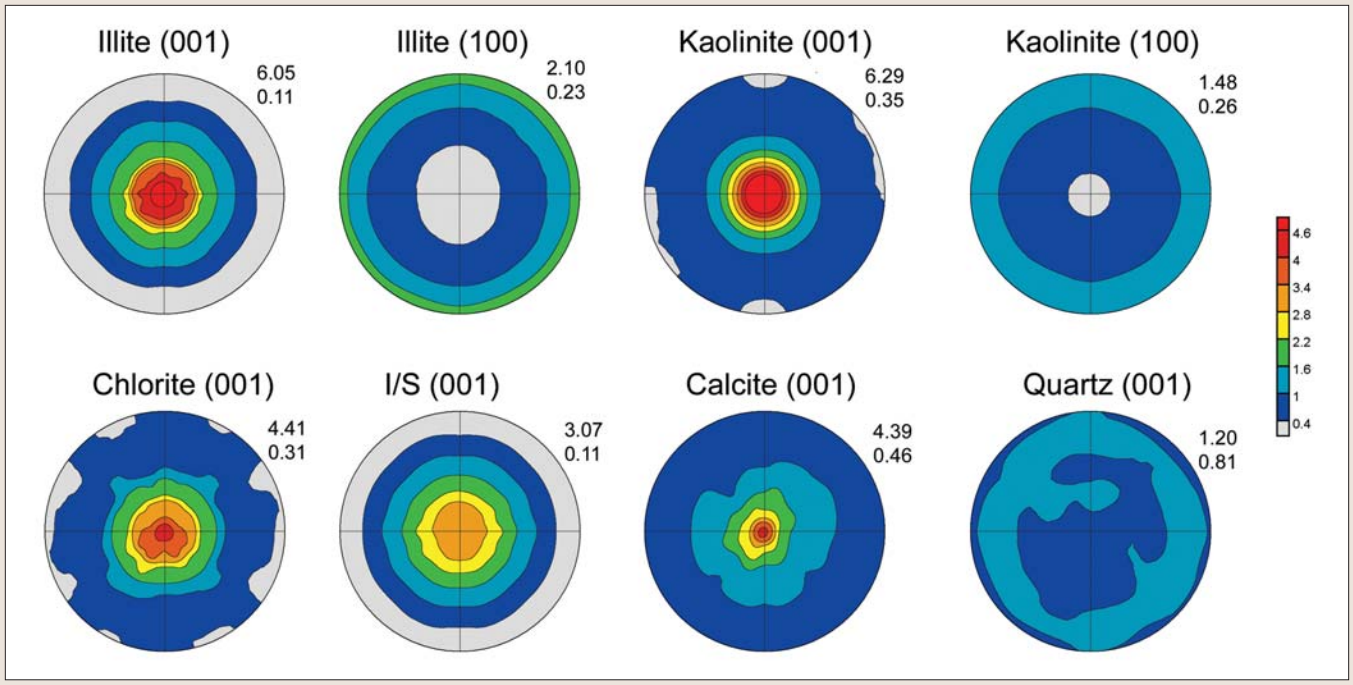

Figure 5. *Pole figures of illite, kaolinite, chlorite, illite/smectite, calcite, and quartz. Equal area projection. Pole densities are expressed in multiples of a random distribution (mrd). The numbers on the top right of each projection are maximum and minimum pole densities (in mrd).*

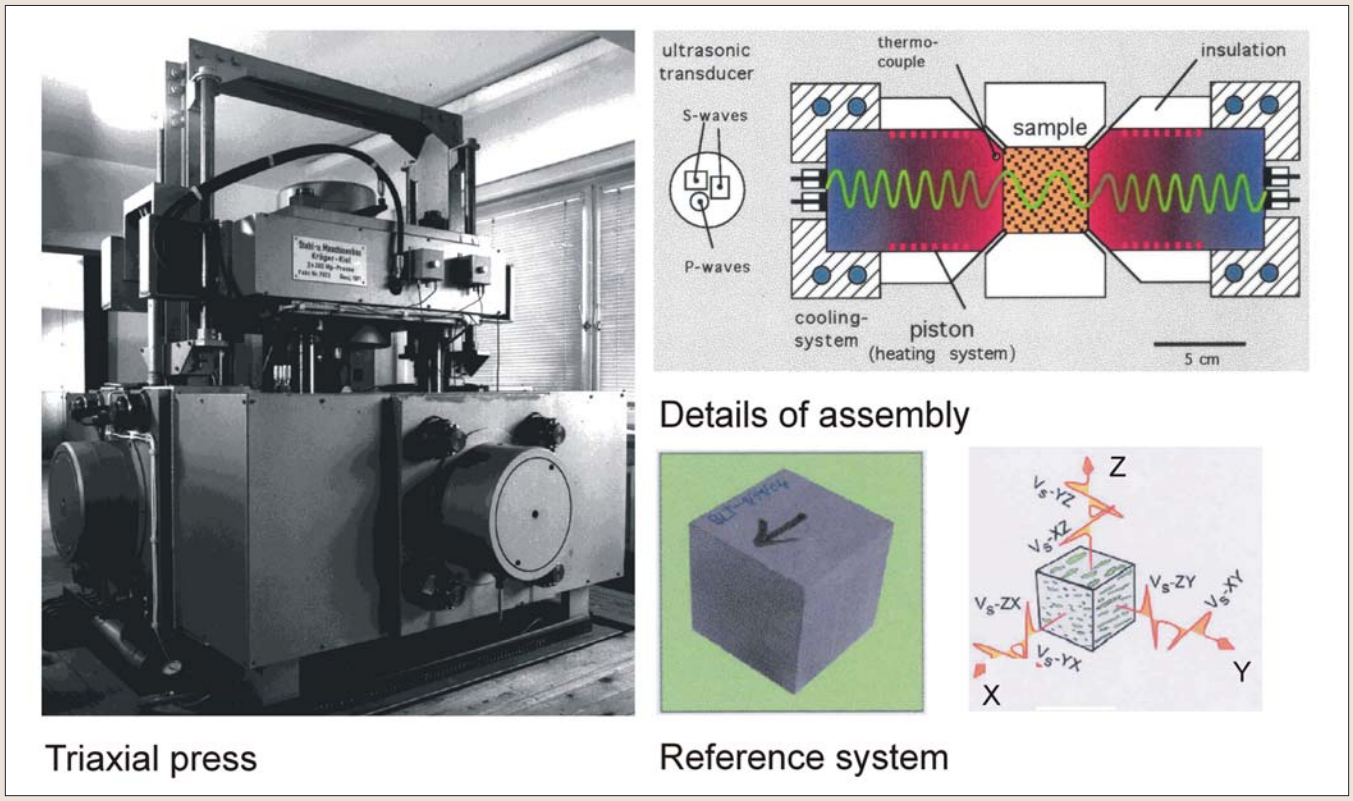

Figure 6. *Multianvil pressure apparatus at Kiel University used for ultrasonic velocity measurements with details of the assembly and a reference system for velocities in the sample cube. Z is perpendicular to the bedding plane.*

of shales, anisotropy of elastic properties has been of great interest because of its significance in seismic prospecting.

On the same sample used for texture analysis, ultrasonic wave velocities were measured in different directions as a function of pressure. A photograph of the triaxial press and a sketch illustrating the transducer-piston-sample assembly are shown in Figure 6. P- and S-wave velocities were measured using the ultrasonic pulse transmission technique with transducers operating at 2 MHz and 1 MHz, respectively. Measurements were done in a multi-anvil pressure apparatus allowing simultaneous measurements of compressional V_P and shear wave velocities V_S in the three orthogonal directions (x, y, and z) that are related to the bedding plane (x and y = parallel to bedding, z = normal to bedding, see Figure 6 for sample reference system). Splitting of shear waves is generally obtained by two sets of orthogo-

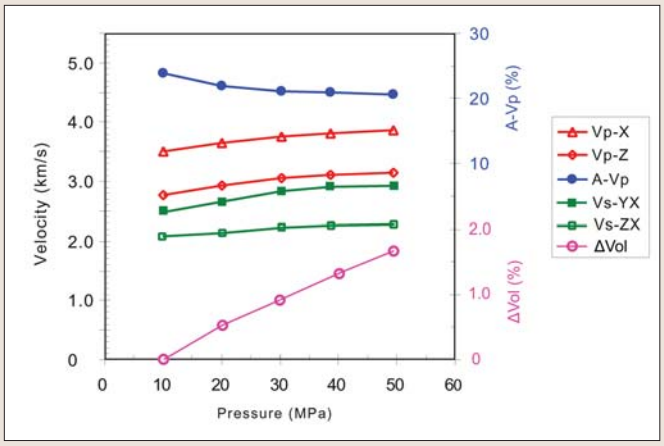

Figure 7. *Experimental ultrasonic P- and S-wave velocities in x, y, and z directions; P-wave anisotropy (A-V_P), and volume change (ΔVol) as functions of pressure.*

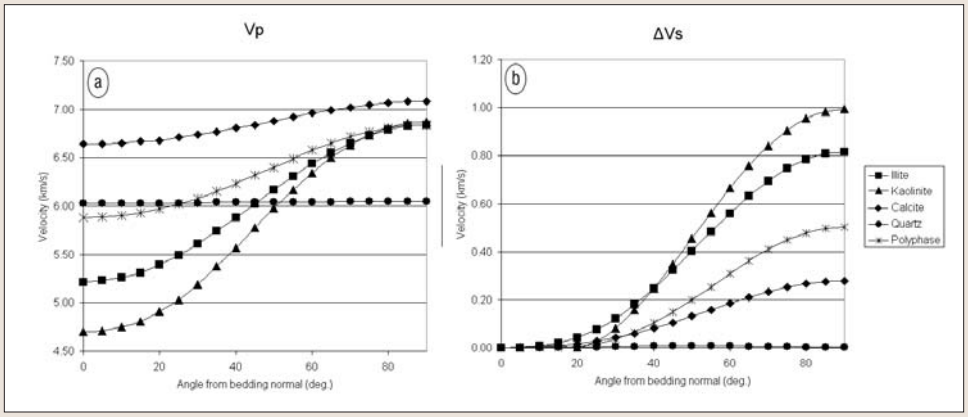

Figure 8. *Calculated P- and S-wave velocities as functions of the angle to the bedding plane. Porosity is not considered in the polyphase average.*

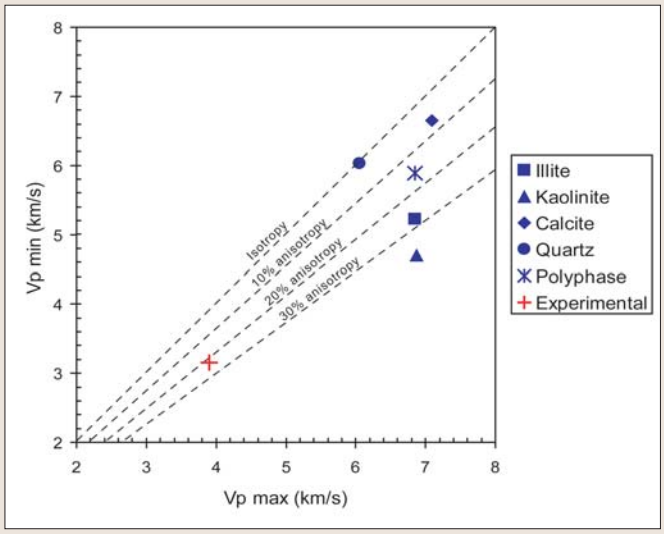

Figure 9. *Experimental (red) and calculated (blue) maximum and minimum P-wave velocities. The lines indicate anisotropy.*

nal polarized shear-wave transducers. The precision of the timing measurements is ± 5 ns, and the timing accuracy is believed to be better than ± .5 %. To ensure that the sample had reached pressure equilibrium, successive readings were taken at time intervals of at least 30 minutes for each pressure step. The length and resulting volume changes of the sample were obtained by the piston displacement.

Measurements of P- and S-wave velocities were done at room temperature on the dry sample at pressures ranging from 10 to 50 MPa. Unfortunately, not all potentially measurable S-wave velocities could be determined, because of some weak signals. Figure 7 presents measured P-wave and S-wave velocities in different structural directions (x, y, and z) as well as the corresponding volume change. The velocity-pressure relations display the well-known nonlinear velocity increase with confining pressure due to progressive closure of microcracks resulting from sample compaction, which is highest normal to the bedding plane. The overall volume change at 50 MPa is 1.7%. *Vp* is highest parallel to the bedding plane (x) and lowest normal to it (z). The significant differences of P-wave velocities measured in the different structural directions indicate a strong velocity anisotropy defined by the percent differences between maximum and minimum velocity with respect to mean velocity: [A=200% (Vmax-Vmin)/(Vmax+Vmin)]. At 50 MPa it is about 20%.

Another measure for anisotropy is shear-wave splitting. A single shear wave propagating through an anisotropic material will be split into approximately two orthogonal polarizations, which travel at different speeds in the same direction. Shear-wave splitting is highest parallel to bedding with the fast split shear wave polarized parallel to the bedding plane. It amounts to 0.58 km/s. Normal to bedding, there is practically no observed shear-wave splitting and the sample is quasi-isotropic for shear waves.

The seismic anisotropy depends on the elastic properties of the aggregate. For metals, ceramics and low-porosity rocks, the elastic properties can be obtained by averaging single crystal properties over the orientation distribution. There are various averaging schemes. The Voigt and Reuss averages provide upper and lower bounds, assuming uniform strain and uniform stress, respectively, throughout the textured aggregate. Arithmetic and geometric means are intermediate. Self-consistent averaging satisfies both stress and strain criteria. We calculated the intrinsic part of aggregate elastic properties due to crystal alignment for Mont Terri shale by averaging single crystal tensors with a geometric mean (illite + illite/smectite, kaolinite, calcite, quartz). Since pole figures are nearly axially symmetric, transverse isotropy was assumed. From aggregate elastic constants and density, we then calculated aggregate phase velocities in different directions using the Christoffel transformation and anisotropies for P-waves and shear-wave splitting. Figure 8 shows the velocity variations as a function of angle to the bedding plane for individual phases of the sample and the polyphase average. Kaolinite is the most anisotropic. Note that, even though calcite is oriented, its contribution to polyphase anisotropy is minimal. The fastest P-wave velocities are in the bedding plane, as is the fastest split shear wave (0.5 km/s); this is close to the value of the experiment. The polycrystal elastic anisotropy of P-waves is 15.1%.

Anisotropies inferred from texture patterns are close to experimental values but experimental ultrasonic velocities are much lower (Figure 9). The reason is that our model only captures one part of the physical characteristics of shale. In

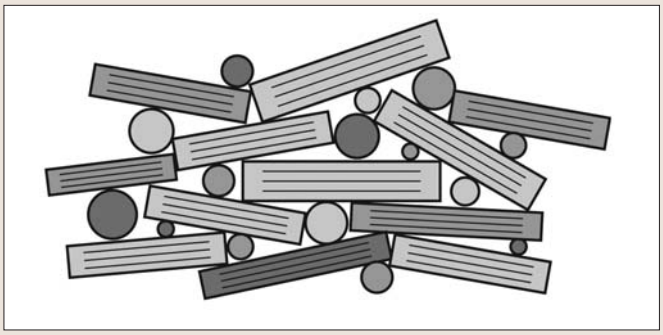

Figure 10. *Sketch of a shale microstructure with intermixed platy and isometric crystals, porosity, and discrete grain contacts.*

shales the system is complicated by significant porosity and only limited grain contacts. Furthermore pores are not equiaxial. The sketch in Figure 10, modified from Hornby et al. (1994), summarizes these contributions to elastic properties and particularly anisotropy. Single-crystal elastic properties of clay minerals are poorly known. In our calculations, experimental values for muscovite (Vaughan and Guggenheim, 1986) have been used for illite and first-principles simulations (Sato et al., 2005) for kaolinite but there are large uncertainties. The apparent high anisotropy for kaolinite is in part due to single crystal constants.

Orientation distributions are an intrinsic part of polycrystal elastic properties and can now be quantified, for example with synchrotron diffraction methods described above for the various phases. This is a well-constrained component. Bulk porosity can be measured but the topology of the pore space and the grain-to-grain contacts are much more uncertain. An empirical model developed by Sayers (1999, 2005) represents the effect of the low-aspect-ratio pores in shales via a normal and shear compliance, and obtains information on these parameters from a comparison of ultrasonic velocity measurements and theoretical predictions. By comparing theory with experiment, Sayers showed that the ratio of the normal to shear compliance of the low-aspect-ratio pores in shales increases with decreasing saturation of the shales studied. It should be noted that in this study all measurements were done on dry samples.

In the future more sophisticated averaging schemes need to combine crystal orientation patterns with pore geometry and distribution as well as particle shape and topology in a comprehensive fashion. Also, ultrasonic velocity measurements on the sample samples should be repeated with pore fluid present to further constrain the influence of porosity. Synchrotron X-rays have been instrumental for obtaining quantitative orientation distributions of all phases. They may also become the method of choice to quantify pore space and particle shape distributions with new techniques of microtomography now being developed. Having determined experimental results for physical properties, we can now explore the influence of other factors on anisotropy of shales.

Suggested reading. "Mont Terri Project—Geology, Paleohydrology and Stress Field of the Mont Terri Region" by Heitzmann and Tripet (Federal Office for Water and Geology, Geology Series 4, Bern, Switzerland). "Anisotropic effective-medium modeling of the elastic properties of shales" by Hornby et al. (GEOPHYSICS, 1994). "Relationship between anisotropy of P- and S-wave velocities and anisotropy of attenuation in serpentinite and amphibolite" by Kern et al. (*Journal of Geophysical Research*, 1997). "Unravelling the multi-stage burial history of the Swiss Molasse Basin: Integration of apatite fission track, vitrinite reflectance, and biomarker isomerisation analysis" by Mazurek et al. (*Basin Research* 2006). "Anisotropy and mechanical properties of Opalinus clay during triaxial deformation in a multianvil apparatus" by Popp and Salzer (*Physical Chemistry of the Earth,* 2007). "First-principles studies on elastic constants of a 1:1 layered kaolinite mineral" by Sato et al. (*American Mineralogist*, 2005). "Stress-dependent seismic anisotropy of shales" by Sayers, (GEOPHYSICS, 1999). "Seismic anisotropy of shales" by Sayers (*Geophysical Prospecting,* 2005). "The Mont Terri rock laboratory, a new international research project in a Mesozoic shale formation, in Switzerland" by Thury and Bossart (*Engineering Geology,* 1999). "Elasticity of muscovite and its relationship to crystal structure" by Vaughan and Guggenheim (*Journal of Geophysical Research,* 1986). "Preferred orientation and elastic anisotropy of illite-rich shale" by Wenk et al. (GEOPHYSICS, 2007). "Preferred orientations and anisotropy in shales: Callovo-Oxfordian shale (France) and Opalinus Clay (Switzerland)" by Wenk et al. (*Clays and Clay Minerals,* in press). *The Rietveld Method* by Young (Oxford, 1993).

Acknowledgements. We are grateful to BGR for providing the sample and to O. Schulze for his assistance in preparing the sample cube. Access to beamline 11-ID-C at APS and help from instrument scientist Yang Ren were invaluable. Special thanks to D. Schulte-Kortnack for his help with the multianvil apparatus. We also appreciate discussions and constructive editorial comments by Dave Dewhurst and Colin Sayers. The project was supported by DOE-BES (DE-FG02-05ER15637) and NSF (EAR-0337006).

Corresponding author: wenk@berkeley.edu